

**Pressure-induced ferromagnet to spin-glass transition in  $\text{Gd}_2\text{Mo}_2\text{O}_7$** I. Mirebeau,<sup>1</sup> A. Apetrei,<sup>1</sup> I. Goncharenko,<sup>1</sup> D. Andreica,<sup>2,3</sup> P. Bonville,<sup>4</sup> J. P. Sanchez,<sup>5</sup> A. Amato,<sup>2</sup> E. Suard,<sup>6</sup> W. A. Crichton,<sup>7</sup> A. Forget,<sup>4</sup> and D. Colson<sup>4</sup><sup>1</sup>Laboratoire Léon Brillouin, CEA-CNRS, CE-Saclay, 91191 Gif-sur-Yvette, France<sup>2</sup>Laboratory for Muon Spin Spectroscopy, Paul Scherrer Institute, 5232 Villigen-PSI, Switzerland<sup>3</sup>Faculty of Physics, Babes-Bolyai University, 400084 Cluj-Napoca, Romania<sup>4</sup>Service de Physique de l'Etat Condensé, CEA-CNRS, CE-Saclay, 91191 Gif-sur-Yvette, France<sup>5</sup>Service de Physique Statistique, Magnétisme et Supraconductivité, CEA-Grenoble, 38054 Grenoble, France<sup>6</sup>Institut Laue Langevin, 6 rue Jules Horowitz, Boîte Postale 156X, 38042 Grenoble, France<sup>7</sup>European Synchrotron Radiation Facility, Boîte Postale 220, 38043 Grenoble, France

(Received 24 May 2006; published 13 November 2006)

$\text{R}_2\text{Mo}_2\text{O}_7$  compounds show a ferromagnetic metal-insulator spin-glass transition tuned by the radius of the rare earth ion  $R^{3+}$ . We have studied  $\text{Gd}_2\text{Mo}_2\text{O}_7$  located on the verge of the transition, by neutron diffraction on a  $^{160}\text{Gd}$  isotopic sample,  $\mu\text{SR}$  and x-ray diffraction using the synchrotron radiation. All measurements were done both at ambient and under applied pressure. At ambient pressure, a ferromagnetic state is observed below the Curie temperature ( $T_C=70$  K). The ordered magnetic moments at 1.7 K are parallel and equal to  $5.7(5) \mu_B$  and  $0.8(2) \mu_B$  for Gd and Mo, respectively. The relaxation rate measured by  $\mu\text{SR}$  evidences strong spin fluctuations below  $T_C$  and down to the lowest temperature (6.6 K). A spin reorientation occurs in the range  $20 \text{ K} < T < T_C$ . The ferromagnetic state is strongly unstable under pressure.  $T_C$  sharply decreases (down to 38 K at 1.3 GPa) and Bragg peaks start to coexist with mesoscopic ferromagnetic correlations. The ordered moments decrease under pressure. At 2.7 GPa long range magnetic order completely breaks down. In this spin-glass state, Gd-Gd spin correlations remain ferromagnetic with a correlation length limited to the fourth neighbor, and Gd-Mo spin correlations turn to antiferromagnetic. The unique combination of three microscopic probes under pressure provides a detailed description of the magnetic transition, crucial for further theories.

DOI: [10.1103/PhysRevB.74.174414](https://doi.org/10.1103/PhysRevB.74.174414)

PACS number(s): 71.30.+h, 71.27.+a, 75.25.+z

**I. INTRODUCTION**

Pyrochlores compounds  $\text{R}_2\text{T}_2\text{O}_7$ , where  $R^{3+}$  and  $T^{4+}$  are rare earth and transition or  $sp$  metal ions, respectively, show geometrical frustration of the first neighbor interactions. This occurs not only for antiferromagnetic interactions between first neighbor Heisenberg moments, but also for ferromagnetic interactions if the neighboring moments are constrained to lie along their local Ising anisotropy axes. This peculiarity of the pyrochlore lattice leads to exotic types of short range magnetic orders, such as spin liquids, spin ices or chemically ordered spin glasses, which are intensively studied.<sup>1,2</sup>

Among the pyrochlores, rare earth molybdenum pyrochlores  $\text{R}_2\text{Mo}_2\text{O}_7$  have attracted special attention since the discovery of a crossover transition from an insulating spin-glass state to a metallic ferromagnetic state, which can be tuned by the rare earth ionic radius.<sup>3,4</sup> The variation of the transition temperature which shows a universal curve for all compounds with mixed rare earth ions, suggests that the dominant mechanism comes from a change in the sign of the Mo-Mo interactions. This change is connected with a change in the band structure, due to the specific energy of Mo  $t_{2g}$  orbitals, situated nearby the Fermi level and well separated from the other bands.<sup>5,6</sup> The insulating state observed at low rare earth ionic radius is attributed to the opening of a Mott-Hubbard gap at the Fermi level, due to strong electronic intrasite interactions.<sup>6</sup> With increasing rare earth ionic radius, Mo-Mo first neighbor interactions seem to evolve from antiferromagnetic, dominated by a superexchange mechanism and frustrated by the geometry, to ferromagnetic, due to a double exchange mechanism.

In the ferromagnetic region, the ferromagnetic alignment of the neighboring Mo moments favors the electronic kinetic energy and leads to a metallic conductivity, with a mechanism similar to that observed in the manganites. The rare earth crystal field anisotropy also plays a role, since it yields a possible source of frustration in the ferromagnetic region. This frustration seems to have important consequences on the conductivity properties. Namely, the  $\text{Nd}_2\text{Mo}_2\text{O}_7$  compound shows a giant abnormal Hall effect at low temperature<sup>7,8</sup> which cannot be explained by the spin-orbit coupling. It is generally admitted that this effect is induced by the spin ice frustration of the  $4f$   $\text{Nd}^{3+}$  spins, transferred to itinerant Mo electrons through  $f-d$  interaction.

$\text{Gd}_2\text{Mo}_2\text{O}_7$  is especially interesting since the Gd ionic radius is situated just above the threshold for the metal insulator transition. This compound was thoroughly investigated by many techniques. Magnetic measurements<sup>9,10</sup> suggest a ferromagneticlike transition at  $T_C$ , with magnetic irreversibilities occurring below. The  $T_C$  values reported by various groups are in the range 40–70 K. Mössbauer measurements<sup>10</sup> show a hyperfine field below the transition and the hyperfine populations are found to be out of thermal equilibrium at 27 mK, indicating that Gd and Mo spin fluctuations are present in the magnetic phase and persist down to very low temperature. Heat capacity measurements<sup>12</sup> show two steplike anomalies, suggesting two magnetic transitions, one at  $T_C$  (70 K) and the other well below (11 K). The transport properties strongly depend on sample preparation. First measurements on powdered samples<sup>11</sup> show a metallic conductivity, with anomalies at  $T_C$  and in the 10–20 K temperature

range. However, more recent data on high purity single crystals<sup>13</sup> show an insulating ground state, which is very sensitive to impurity doping. In contrast with  $\text{Nd}_2\text{Mo}_2\text{O}_7$ , the Hall conductivity<sup>8</sup> shows the behavior of a conventional ferromagnet, as expected for Heisenberg-like  $\text{Gd}^{3+}$  moments ( $4f^7$ ) without orbital angular momentum. An investigation by infrared (IR) spectroscopy<sup>13</sup> shows the presence of a very small Mott-Hubbard gap of 20 meV, about ten times smaller than in the neighboring insulating compounds (170 and 250 meV for Dy and Ho, respectively). The concomitant changes in the optical, magnetic, and transport properties suggest a quantum phase transition around  $\text{Gd}_2\text{Mo}_2\text{O}_7$ , opening the possibility to tune the transition by pressure and/or magnetic field. Magnetic measurements under pressure<sup>14,15</sup> and recent resistivity measurements<sup>16</sup> demonstrated this possibility at a macroscopic level.

Up to now, there was no characterization of the type of magnetic order and magnetic fluctuations in  $\text{Gd}_2\text{Mo}_2\text{O}_7$ . This is especially due to the huge absorption of natural Gd, which makes neutron scattering experiments extremely difficult. We present here an investigation of the magnetic order and magnetic fluctuations in  $\text{Gd}_2\text{Mo}_2\text{O}_7$ , by combining neutron diffraction on a  $^{160}\text{Gd}$  isotopic sample with  $\mu\text{SR}$  experiments. We show that a ferromagnetic collinear order is indeed stabilized well below  $T_C$ , but that it coexists with low temperature fluctuations. At intermediate temperatures ( $20\text{ K} < T < T_C$ ) a reorientation of the magnetic moments occurs.

We also studied the sensitivity of the magnetic state in  $\text{Gd}_2\text{Mo}_2\text{O}_7$  to applied pressure by neutron diffraction and  $\mu\text{SR}$ . The pressure induced changes of the crystal structure and lattice constant were checked by x-ray diffraction using the synchrotron radiation. We observe a pressure induced magnetic transition, which can be fully characterized using this unique combination of three microscopic probes. We show that the ferromagnetic state is highly unstable under pressure: a rather small pressure of 1.3 GPa yields a decrease of the Curie temperature by a factor of two. At 2.7 GPa, long range ferromagnetic order has fully disappeared. Our results demonstrate that the changes in magnetism induced by pressure are equivalent to those induced by chemical pressure ( $R$  substitution). They confirm at a microscopic level the conclusions inferred from the magnetization.<sup>14</sup> Therefore, keeping the same sample, a quantitative analysis of the neutron and muon data allows us to follow the evolution of the spin correlations and fluctuations throughout the transition.

The paper is organized as follows. In Sec. II, we describe the sample characterization, bulk magnetic properties, and crystal structure. In Sec. III, we describe the magnetic state at ambient pressure, studied by neutron diffraction and  $\mu\text{SR}$  as a function of temperature. In Sec. IV, we describe the evolution of the magnetic state under pressure from x-ray, neutron and  $\mu\text{SR}$  experiments. In Sec. V, we discuss the results in comparison with other experimental data and current theories.

## II. CRYSTAL STRUCTURE AND BULK MAGNETIC PROPERTIES

Powdered  $\text{Gd}_2\text{Mo}_2\text{O}_7$  samples were synthesized following the procedure given in Ref. 3. We used  $\text{Gd}_2\text{O}_3$  and  $\text{MoO}_2$

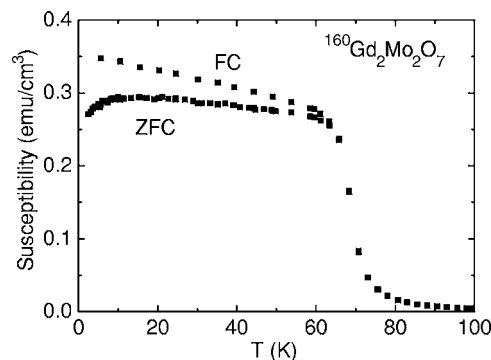


FIG. 1. Magnetic susceptibility measured in a static field of 50 G, in the zero field cooling (ZFC) and field cooling (FC) processes.

oxides as starting materials. The synthesis was made in an argon atmosphere without any excess of Mo, but with Ti/Zr chips to absorb oxygen traces. Samples were heated up to 1370 °C during 6 h. Two annealings at least were necessary to obtain the sample in pure form. A sample of 1 g with natural Gd was prepared for synchrotron and  $\mu\text{SR}$  experiments and a sample of 0.5 g with isotopically enriched  $^{160}\text{Gd}$  was used for the neutron experiments. Both samples were characterized by x-ray diffraction, showing that they are single phase.

The dc magnetization of the two samples were recorded in a superconducting quantum interference device (SQUID) magnetometer with a static field of 50 G. Both show a rather broad Curie transition, as already reported in the literature. In the  $^{160}\text{Gd}$  sample (Fig. 1), the transition occurs in a temperature range  $\Delta(T) = \pm 7\text{ K}$ , with a  $T_C$  value of 70 K defined as the inflexion point in the susceptibility curve. In the sample with natural Gd, we get  $T_C = 72\text{ K}$  and  $\Delta(T) = \pm 5\text{ K}$ . Below the transition we observe irreversibilities of the susceptibility depending on the cooling process, zero field cooling (ZFC) or field cooling (FC). In both samples they occur just below the Curie transition. The FC susceptibility linearly increases with decreasing temperature, whereas the ZFC susceptibility flattens and starts to drop below about 14 K. This drop suggests a blocking of domain walls mobility, possibly related to the spin reorientation discussed below.

The crystal structure of  $\text{Gd}_2\text{Mo}_2\text{O}_7$  was investigated at 300 K by combining powder x-ray and neutron diffraction, the neutron pattern being measured in the high resolution-high flux diffractometer D2B of the Institute Laue Langevin with an incident wavelength of 1.594 Å in the high intensity version. In order to decrease the residual absorption, the sample was placed in a hollow vanadium cylindrical container. In the refinement, we made a specific absorption correction, taking into account the container geometry,<sup>17</sup> the neutron wavelength, and the isotopic composition of the sample. The linear absorption coefficients were estimated to  $\mu = 6.3$  and  $4.1\text{ cm}^{-1}$  for D2B and D20, respectively.

The Rietveld refinement of the D2B diffraction pattern (Fig. 2) was made using the crystallographic programs of the Fullprof suite.<sup>18</sup> We took the diffraction pattern from the vanadium container into account as a second phase. The refinement ( $R_B = 8.9\%$ ,  $R_F = 5.9\%$ ) confirmed the structural model

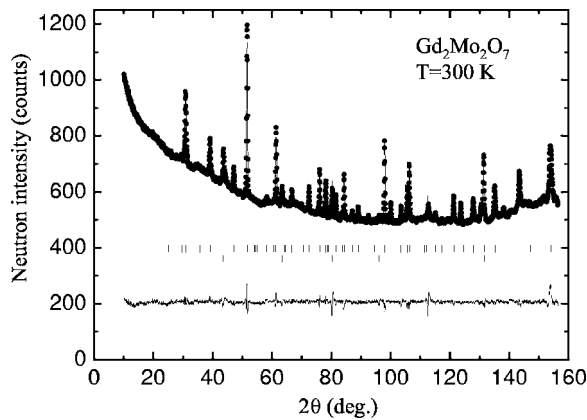


FIG. 2. Neutron diffraction pattern of  $\text{Gd}_2\text{Mo}_2\text{O}_7$  measured at 300 K (paramagnetic phase) on the D2B powder diffractometer, with an incident neutron wavelength of 1.594 Å. Upper and lower tick marks show the Bragg peak positions of the sample and vanadium sample holder, respectively. Solid lines show the calculated pattern ( $R_B=8.9\%$ ) and the difference spectrum.

for a stoichiometric pyrochlore with space group  $Fd\bar{3}m$ , yielding a lattice constant  $a=10.3481(2)$  Å and an oxygen position parameter  $u=0.3342(2)$  at room temperature. These results agree with previous determinations from synchrotron radiation x-ray powder diffraction.<sup>4</sup>

### III. MAGNETIC STATE AT AMBIENT PRESSURE

#### A. Magnetic neutron diffraction

Neutron diffraction patterns were recorded between 1.7 and 90 K on the high flux diffractometer D20 of the Institute Laue Langevin with an incident wavelength 2.419 Å, with the same sample and sample holder as for D2B. Absorption corrections were made as above. Magnetic diffraction patterns were obtained by subtracting a spectrum at 90 K just above the transition. The magnetic pattern at 1.7 K is shown in Fig. 3. The magnetic peaks have  $hkl$  indices of the face centered cubic lattice. The (200) and (220) peaks, where there is no chemical contribution from Gd and Mo ions in the pyrochlore structure (due to extinction from the  $Fd\bar{3}m$  space group and special Gd-Mo positions, respectively) are also absent in the magnetic pattern. We refined the magnetic patterns using the Fullprof suite.<sup>18</sup> At 1.7 K, we obtain a good refinement assuming a collinear ferromagnetic structure (magnetic factor  $R_B=11.3\%$ , Fig. 3). The Mo and Gd moments orient along the same direction, with a ferromagnetic coupling. According to the  $^{155}\text{Gd}$  Mössbauer measurements,<sup>10</sup> the angle between the Gd moment and the  $\langle 111 \rangle$  axis is close to  $54^\circ$ . This strongly suggests that the Gd and Mo moments lie along a  $\langle 100 \rangle$  axis.

With increasing temperature the intensities of the magnetic Bragg peaks start to decrease, but the (111) peak decreases much more rapidly than the high angle peaks (Fig. 4). It disappears around 50 K whereas the other peaks persist up to 70 K. Concomitantly, the magnetic intensities calculated within the collinear ferromagnetic model start to dis-

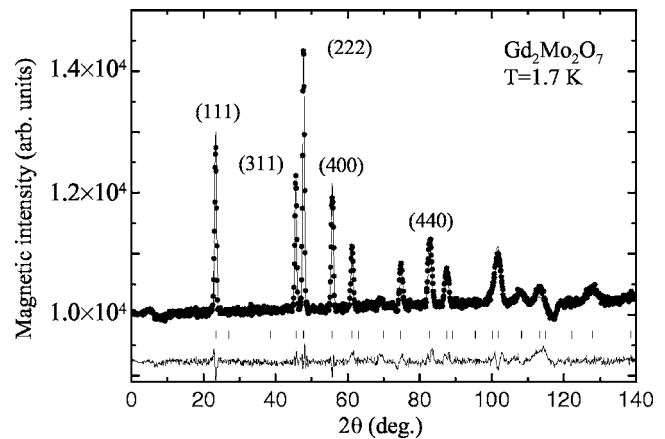


FIG. 3. Magnetic neutron diffraction pattern of  $\text{Gd}_2\text{Mo}_2\text{O}_7$  measured at 1.7 K on the D20 powder diffractometer, with an incident neutron wavelength of 2.419 Å. A pattern measured at 90 K (above  $T_C$ ) was subtracted. Tick marks show the Bragg peak positions. Solid lines show the pattern calculated with the collinear ferromagnetic model ( $R_B=11.3\%$ ) and the difference spectrum.

agree with the experimental data (inset Fig. 4,  $R_B=39\%$  at 40 K).

The refinements exclude a zero ordered moment on either the Gd or Mo sublattice. A global change of orientation of both Gd and Mo sublattices is also excluded since it would not change the magnetic diffraction pattern of a powdered cubic structure. The observed anomaly is therefore attributed to a decoupling of  $\text{Gd}^{3+}$  and  $\text{Mo}^{4+}$  moments above 20 K, yielding noncollinear moments in the Gd (and possibly Mo) sublattice. Unfortunately, a precise determination of this noncollinearity is hampered by the high symmetry of the crystal structure, the presence of eight independent moments in the unit cell, and the dominant ferromagnetic character.

To search for noncollinear structures, we first performed a symmetry analysis<sup>19,20</sup> using the program BasIreps,<sup>21</sup> searching for all  $\mathbf{k}=0$  structures corresponding to irreducible representation of the  $I4_1/amd$  space group, the highest symme-

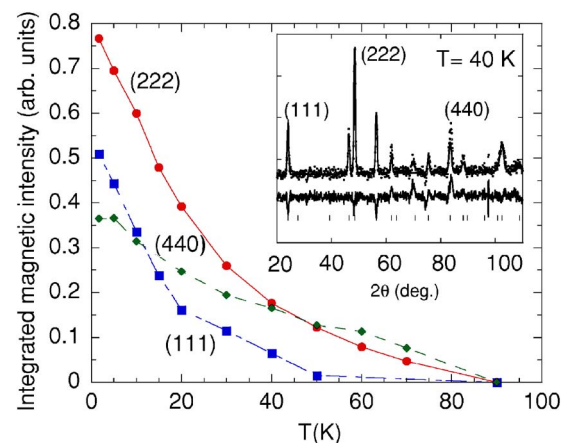


FIG. 4. (Color online) Integrated intensity of several magnetic Bragg peaks in  $\text{Gd}_2\text{Mo}_2\text{O}_7$ , measured versus temperature on D20. The intensities are scaled to the intensity of the (222) nuclear peak at 90 K. In the inset the magnetic diffraction pattern at 40 K.

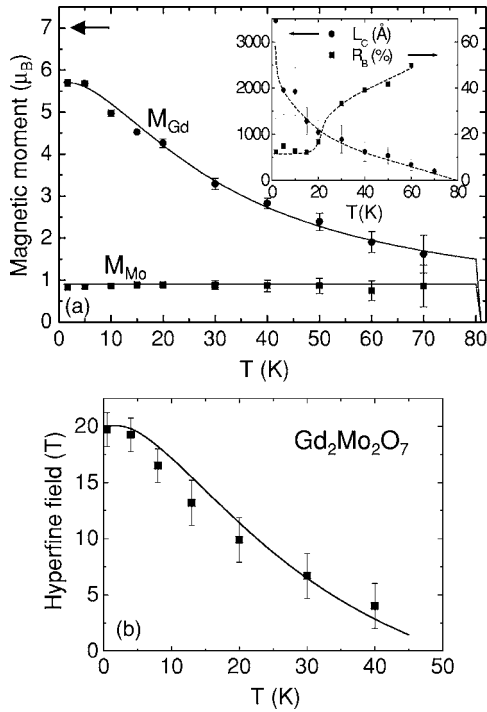


FIG. 5. (a) Temperature dependence of the ordered moments  $M_{\text{Gd}}$  (circles) and  $M_{\text{Mo}}$  (squares) in  $\text{Gd}_2\text{Mo}_2\text{O}_7$  deduced from refinements of the neutron data in the collinear ferromagnetic model. Errors bars are given by Fullprof. The arrow shows the Gd free ion value of  $7 \mu_B$ . The solid line for Gd is a fit with a Brillouin function (see text). In the inset, the magnetic correlation length  $L_c$  deduced from the peak linewidth (dots, see text) and the magnetic factor  $R_B$  (squares) versus temperature. Dashed lines are guides to the eye. (b) Thermal variation of the  $^{155}\text{Gd}$  hyperfine field in  $\text{Gd}_2\text{Mo}_2\text{O}_7$ , from Ref. 10. The line is a fit to the sum of a contact hyperfine field, proportional to the Gd moment, and of a transferred field, proportional to the Mo moment, and thus temperature independent.

try group allowing ferromagnetism. We also checked noncollinear structures predicted by theory, assuming either anisotropic or dipolar interactions.<sup>22,23</sup> Finally, we explored small deviations from the ferromagnetic collinear case using the simulated annealing process available in Fullprof.<sup>18</sup> Whatever the procedure, we could not improve the quality of the refinement significantly with respect to the collinear ferromagnetic model. We conclude that a noncollinearity of the Gd/Mo ordered moments indeed occurs above 20 K, although we cannot determine its nature presently. We also notice a slight change of the peak linewidth, showing that the magnetic correlation length increases with decreasing  $T$  in this temperature range [inset Fig. 5(a)]. The correlation length was deduced from the Fullprof refinement of the Lorentzian contribution to the peak profile, taking into account the instrumental resolution parameters, and using a Thompson-Cox-Hastings pseudo-Voigt profile function for the lineshape.<sup>18</sup>

The temperature dependence of the ordered magnetic moments deduced from refinements in the collinear ferromagnetic model is plotted in Fig. 5(a). At 1.7 K, the moment values deduced from the refinement are  $5.70(8) \mu_B$  and  $0.82(5) \mu_B$  for Gd and Mo, respectively. Considering the un-

certainty on the scale factor between nuclear and magnetic scattering due to the absorption correction, we estimate the ordered magnetic moments in absolute scale with a larger error bar, namely  $5.7(5) \mu_B$  and  $0.8(2) \mu_B$  for  $\text{Gd}^{3+}$  and  $\text{Mo}^{4+}$  ions, respectively. The ordered  $\text{Gd}^{3+}$  moment is reduced with respect to the free ion value of  $7 \mu_B$ . The ordered  $\text{Mo}^{4+}$  moment is also much smaller than the value of  $2 \mu_B$  expected assuming a ionic description ( $4d^2 t_{2g}$  state with  $S = 1$  and  $g = 2$ ). The calculated ordered moment per formula unit of  $13(1) \mu_B$  is significantly smaller than the saturated value of  $16.8 \mu_B$  obtained at 2 K in a high field of 14 T.<sup>16</sup> Since we do not expect any strong reduction of the free ion values from crystal field effects (the  $\text{Gd}^{3+}$  moment has no orbital contribution), the reduced moment values should be associated with the low temperature fluctuations. This is also supported by the  $\mu\text{SR}$  experiments, as discussed in the next section.

In Fig. 5(a), we show  $M_{\text{Gd}}(T)$  fitted by a Brillouin function  $B_{7/2}$ , assuming that the Gd ions are submitted to a molecular field coming from the Mo ions. As the Mo spontaneous moment is practically temperature independent up to  $T_C$ , we assumed the molecular field  $H_{\text{ex}}$  is constant up to 80 K and vanishes above. The fit in Fig. 5(a) is obtained with  $H_{\text{ex}} = 10.8 \text{ T}$ .

The thermal variation of the Gd moment has also been inferred from the  $^{155}\text{Gd}$  Mössbauer data in  $\text{Gd}_2\text{Mo}_2\text{O}_7$  in Ref. 10, assuming that the Gd moment is proportional to the hyperfine field. Comparison with the present neutron data shows a clear disagreement: the Mössbauer derived values fall much more rapidly than the neutron values as temperature increases. So we propose another interpretation of the Mössbauer data: the measured hyperfine field  $H_{\text{hf}}$  is assumed to be the sum of a contact hyperfine field, proportional to the Gd moment, and of a transferred hyperfine field  $H_{\text{tr}}$  coming from the polarization of the conduction band by the Mo moments (Refs. 24 and 25):

$$H_{\text{hf}}(T) = |AM_{\text{Gd}}(T) + H_{\text{tr}}|. \quad (1)$$

The sign of  $H_{\text{tr}}$  cannot be obtained by the Mössbauer data. The transferred field is proportional to the Mo moment, and it is thus temperature independent up to  $T_C$ . In Fig. 5(b), we have represented the hyperfine field data from Ref. 10 and the fit to the above formula, where  $M_{\text{Gd}}(T)$  is calculated using the Brillouin function as above. The fit yields a contact hyperfine constant  $A = 5.8 \text{ T}/\mu_B$  and a transferred field  $H_{\text{tr}} = -13 \text{ T}$ . The sign of the latter is opposite to that of the contact term, which can occur in intermetallic Gd compounds with  $3d$  or  $4d$  metals.<sup>24,25</sup> Above 40 K, the measured hyperfine field is below 4 T, with a large error bar. The above law predicts that  $H_{\text{hf}}(T)$  shows a minimum at 50 K (not shown), which could not be observed due to the small hyperfine field values. According to this picture,  $\text{Gd}_2\text{Mo}_2\text{O}_7$  is an example where the measured  $^{155}\text{Gd}$  hyperfine field is not proportional to the spontaneous Gd moment.

## B. $\mu\text{SR}$ measurements

$\mu\text{SR}$  measurements at ambient pressure were performed at the Swiss Muon Source at the Paul Scherrer Institute (Vil-

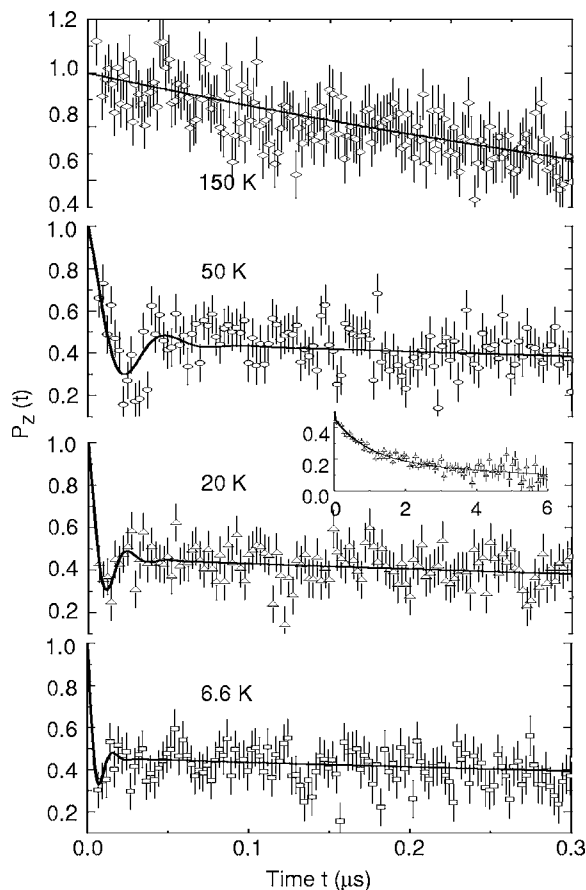


FIG. 6. Muon spin depolarization function  $P_Z(t)$  in  $\text{Gd}_2\text{Mo}_2\text{O}_7$  measured on the GPS beam line at several temperatures (ambient pressure). Lines are fits as described in text. The inset shows the depolarization function in an extended time range for  $T=20$  K. The apparent oscillations at 6.6 K arise from noise in the data.

ligen, Switzerland) on the GPS instrument in the temperature range 6.6–300 K. Selected  $\mu\text{SR}$  spectra are shown in Fig. 6. Above  $T_C$ , the relaxation function  $P_Z(t)$  shows an exponential like decay:  $P_Z(t) = \exp(-\lambda_Z t)$ . Below  $T_C$ ,  $P_Z(t)$  shows a rapidly damped oscillation at early times which is readily attributed to the presence of magnetic order. An exponential decay is also observed at long time scales in the ordered phase, showing that spin fluctuations persist down to the lowest temperature.

Below  $T_C$ , the relaxation function  $P_Z(t)$  was fitted by the equation:

$$P_Z(t) = [\exp(-\lambda_Z t) + 2 \exp(-\lambda_T t) \cos(\gamma_\mu \langle B_{loc} \rangle t)] / 3. \quad (2)$$

This equation is expected to hold in the magnetically ordered phase of a powder sample.<sup>26</sup> The first term corresponds to the depolarization by spin fluctuations with the longitudinal relaxation rate  $\lambda_Z$ , whereas the second term reflects the precession of the muon spin in the average local field  $\langle B_{loc} \rangle$  at the muon site.  $\gamma_\mu$  is the muon gyromagnetic ratio. The transverse relaxation rate  $\lambda_T$  can have both static and dynamical character. In the high temperature limit, when the rate of fluctuations of  $\text{Gd}^{3+}$  and  $\text{Mo}^{4+}$  moments is much larger than the coupling between the muon spin and the elec-

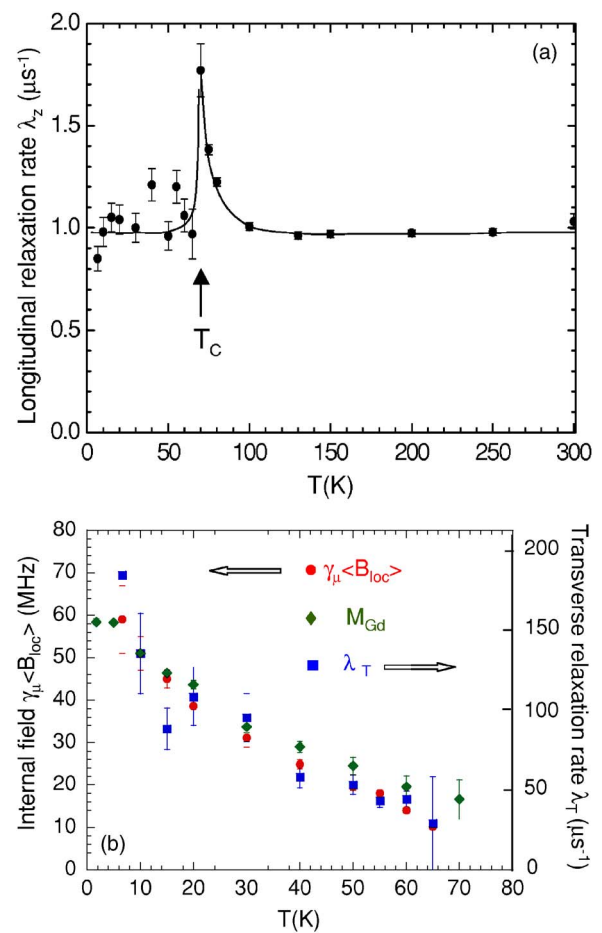


FIG. 7. (Color online) From  $\mu\text{SR}$  measurements in  $\text{Gd}_2\text{Mo}_2\text{O}_7$ . (a) Temperature dependence of the longitudinal relaxation rate  $\lambda_Z$ . The solid line is a guide to the eye. (b) Temperature dependence of  $\gamma_\mu \langle B_{loc} \rangle$  (with  $\gamma_\mu$  the muon gyromagnetic ratio),  $\lambda_T$  and  $M_{\text{Gd}}$  (scaled).

tronic spins, one gets  $\langle B_{loc} \rangle = 0$  and  $\lambda_T = \lambda_Z$ . Then the above equation reduces to a simple exponential  $P_Z(t) = \exp(-\lambda_Z t)$ . This simple function was used to fit the data above  $T_C$ .

In a standard ferromagnet, the longitudinal relaxation rate  $\lambda_Z$  shows a cusp at the critical temperature, then decreases with decreasing temperature below  $T_C$  and tends to zero as  $T \rightarrow 0$  (a  $T^2$  behavior is expected for instance from Raman two magnon processes).<sup>27</sup> In  $\text{Gd}_2\text{Mo}_2\text{O}_7$ ,  $\lambda_Z$  shows a cusp at  $T_C$ , but does not decrease below [Fig. 7(a)]. It keeps a high value close to that in the paramagnetic region down to the lowest measured temperature of 6.6 K, with possibly a very small bump below  $T_C$ , which needs to be confirmed. This abnormal behavior reflects the presence of strong spin fluctuations coexisting with the magnetic order, which seem to persist as  $T \rightarrow 0$  in contrast with standard spin waves. Such peculiar fluctuations have already been observed by  $\mu\text{SR}$  in several geometrically frustrated magnets with a pyrochlore lattice. They were seen in spin liquids<sup>28,29</sup> like  $\text{Tb}_2\text{Ti}_2\text{O}_7$  and  $\text{Yb}_2\text{Ti}_2\text{O}_7$ , as well as in ordered compounds<sup>29–31</sup> like  $\text{Gd}_2\text{Sn}_2\text{O}_7$  and  $\text{Tb}_2\text{Sn}_2\text{O}_7$ . In all cases, the longitudinal relaxation rate saturates in the lowest  $T$  range (to values around  $1 \mu\text{s}^{-1}$ ), as here for  $\text{Gd}_2\text{Mo}_2\text{O}_7$ .

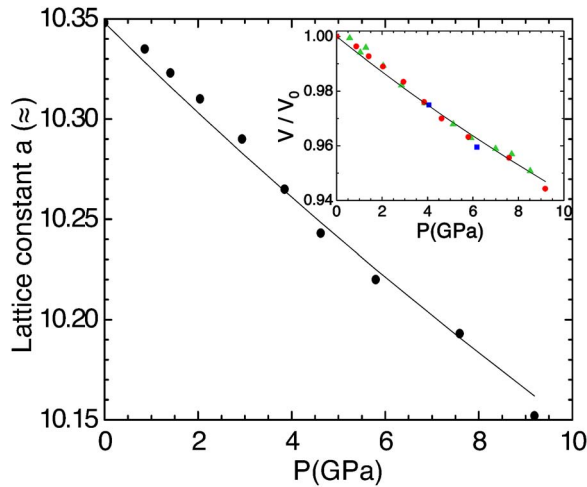


FIG. 8. (Color online) Variation of the lattice constant  $a$  versus pressure at ambient temperature. In the inset the relative volume  $V/V_0$  is plotted versus pressure up to 10 GPa for three samples:  $\text{Gd}_2\text{Mo}_2\text{O}_7$  (circles),  $\text{Tb}_2\text{Mo}_2\text{O}_7$  with  $a_0 < a_c$  (squares), and  $(\text{Tb}_{0.8}\text{La}_{0.2})_2\text{Mo}_2\text{O}_7$  with  $a_0 > a_c$  (triangles). Solid lines are fits to the Murnaghan equation.

The transverse relaxation rate  $\lambda_T$  is up to two orders of magnitude larger than  $\lambda_Z(T)$ . It smoothly increases below  $T_C$  and scales with the average local field  $\langle B_{loc} \rangle$  as temperature varies. This leads us to assign  $\lambda_T$  mainly to the width of the distribution of local fields. We notice that both quantities also scale with the ordered moment  $M_{\text{Gd}}(T)$  determined by neutron diffraction [Fig. 7(b)]. This suggests that the local field seen by the muon mostly comes from the  $\text{Gd}^{3+}$  ions with much larger moments, although more localized, than the  $\text{Mo}^{4+}$  ones. Our current neutron and  $\mu\text{SR}$  data in the  $(\text{Tb}, \text{La})_2\text{Mo}_2\text{O}_7$  series<sup>33</sup> as well as previous  $\mu\text{SR}$  data in  $\text{Tb}_2\text{Mo}_2\text{O}_7$  and  $\text{Y}_2\text{Mo}_2\text{O}_7$  spin glasses<sup>32</sup> support this interpretation, showing that the static internal field is about ten times higher in  $\text{Tb}_2\text{Mo}_2\text{O}_7$ , with both  $\text{Tb}^{3+}$  and  $\text{Mo}^{4+}$  moments, than in  $\text{Y}_2\text{Mo}_2\text{O}_7$  where only  $\text{Mo}^{4+}$  moments are involved.

#### IV. THE PRESSURE INDUCED STATE

##### A. Crystal structure under pressure: X-ray diffraction

X-ray diffraction under pressure using the synchrotron radiation was performed at room temperature on the ID27 beam line of ESRF, in the pressure range 0–10 GPa, with an incident wavelength of 0.3738 Å. We used a diamond anvil cell and an ethanol-methanol mixture as the pressure transmitting medium. The crystal structure remains cubic with a  $Fd\bar{3}m$  space group in the whole measured pressure range.

The evolution of the lattice constant  $a$  versus pressure is shown in Fig. 8. From Ref. 3, one estimates the critical lattice constant for the ferromagnetic spin-glass transition to be  $a_c = 10.327(5)$  Å (critical ionic radius  $r_c = 1.047$  Å). Besides  $\text{Gd}_2\text{Mo}_2\text{O}_7$ , we also studied two samples under pressure for comparison, namely  $\text{Tb}_2\text{Mo}_2\text{O}_7$ , an insulating spin glass with  $a_0 = 10.3124(7)$  Å, smaller than  $a_c$ , and  $(\text{Tb}_{0.8}\text{La}_{0.2})_2\text{Mo}_2\text{O}_7$  with  $a_0 = 10.3787(8)$  Å greater than  $a_c$ . In the studied pres-

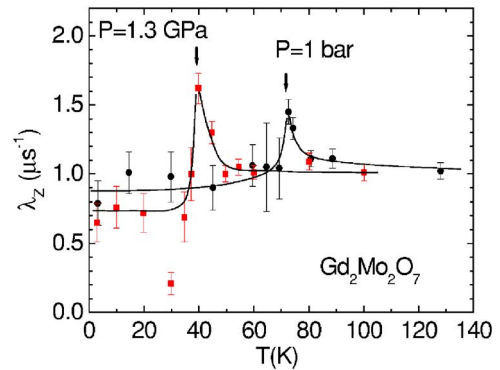


FIG. 9. (Color online) Temperature dependence of the relaxation rate  $\lambda_Z$ , with the  $\text{Gd}_2\text{Mo}_2\text{O}_7$  sample in the pressure cell. Data were measured on the GPD instrument: ambient pressure (circles) and  $P=1.3$  GPa (squares). Solid lines are guides to the eye.

sure range, we found the same variation of the relative volume  $V/V_0$  (where  $V_0$  is the unit cell volume at ambient pressure) for all compounds. The equation of state was fitted to the Murnaghan equation  $V/V_0 = (PB_1/B_0 + 1)^{-1/B_1}$ , yielding a bulk modulus  $B_0 = 148(3)$  GPa. The pressure derivative of the bulk modulus was fixed at a reasonable value ( $B_1 = 4.5$ ).

Knowing the evolution of the lattice constant under pressure enables us to compare the pressure induced state in  $\text{Gd}_2\text{Mo}_2\text{O}_7$  with the ambient pressure state in  $\text{R}_2\text{Mo}_2\text{O}_7$  compounds with a smaller lattice constant. As discussed in the last section, the different experimental determinations of the critical pressure for  $\text{Gd}_2\text{Mo}_2\text{O}_7$  lie in the pressure range 0.6–2.4 GPa.

We notice that the quality of the experimental data was not sufficient to refine the oxygen parameter due to texture effects and/or nonisotropic powder averaging. So we cannot determine the pressure dependence of the Mo-O-Mo bond angle.

##### B. Change of the transition temperature: $\mu\text{SR}$

Muon spin rotation measurements under pressure were performed on the GPD instrument of the Paul Scherrer Institute, using high energy incident muons to penetrate the pressure cell. The sample was mounted in a piston cylinder cell inserted in a cryostat. The pressure transmitting medium was a 1-1 mixture of isopropyl alcohol and *N*-pentane. The signal from the pressure cell (about 70% of the total asymmetry) was fitted by a Gaussian Kubo-Toyabe depolarization function. The sample was first measured in the pressure cell at ambient pressure in the  $T$  range 3.2–130 K, then the cell was pressurized and the experiment repeated. The pressure was determined by measuring the superconducting transition of an indium wire inside the pressure cell, yielding a value of 1.3 GPa. Below  $T_C$  it was difficult to extract any information from the  $\mu\text{SR}$  spectra at small times (the 2/3 term), due both to the large background of the pressure-cell and to the fast depolarization of the 2/3 term. Hence, below  $T_C$  we fitted only the 1/3 term with an exponential depolarization function. Figure 9 compares the temperature dependence of the

relaxation rate at ambient pressure and under 1.3 GPa. The sharp peak in  $\lambda_z(T)$  clearly moves towards lower temperatures under pressure. It reflects a very strong decrease of the transition temperature—from 70 to 38 K, when the pressure increases from ambient pressure to 1.3 GPa.

### C. Change of the spin correlations: Magnetic neutron diffraction

Neutron diffraction measurements under pressure were performed on the spectrometer G6-1 of the Laboratoire Léon Brillouin with an incident wavelength of 4.741 Å, in the high pressure version.<sup>34</sup> The sample was loaded in a sapphire anvil cell with 80% in volume of Al powder. The Al powder was used as a pressure transmitting medium, which ensures a pressure homogeneity within  $\pm 5\%$ , without bringing additional Bragg peaks. It also decreases the sample absorption. Measurements were performed at pressures 0.5, 1.2, 1.9, and 2.7 GPa, between 1.5 and 90 K. Pressure was measured by the ruby fluorescence technique. The magnetic diffraction patterns were obtained by subtracting a pattern at 90 K (paramagnetic phase). The magnetic intensity was scaled to the integrated intensity of the (222) Bragg peak. This procedure allows us to compare diffraction patterns measured at different pressures and temperatures.

Figure 10(a) shows magnetic diffraction patterns at 1.2 GPa. The pattern at 1.5 K shows that magnetic long range (LRO) and short range (SRO) orders coexist in the sample. Small Bragg peaks are clearly visible, with a width limited by the experimental resolution. An intense scattering is also observed at low  $q$  values. This small angle neutron scattering (SANS), which was absent in the ambient pressure data, shows the onset of ferromagnetic correlations with a mesoscopic length scale. With increasing temperature, the (111) peak disappears at about 20 K, whereas the (222) peak vanishes at a higher temperature close to 38 K, the transition temperature determined by  $\mu$ SR for this pressure. It suggests that the spin reorientation observed in the ordered state at ambient pressure still persists under pressure. The short range ferromagnetic correlations persist slightly above the transition.

At 1.9 GPa, a very small ordered component remains at the Bragg positions. At 2.7 GPa, the magnetic Bragg peaks have completely disappeared, and only magnetic short range order is present [Fig. 10(b)]. Short range magnetic correlations are clearly shown at 1.5 K, yielding a strongly modulated magnetic background. Here, the SANS signal coexists with a diffuse peak centered around  $1.1 \text{ \AA}^{-1}$ . With increasing temperature, the diffuse peak flattens and vanishes around 20 K, whereas the ferromagnetic correlations persist up to 40 K.

In Fig. 11(a), we compare diffraction patterns at 1.5 K for several pressures. With increasing pressure, the decrease of the Bragg intensity coincides with the growing of the diffuse magnetic peak, showing that the relative contributions of SRO and LRO vary in opposite way. The SANS signals flattens with increasing either  $T$  or  $P$ , showing that the ferromagnetic correlation length decreases.

To analyze the pressure data we proceeded as follows. The long range magnetic order was analyzed within the col-

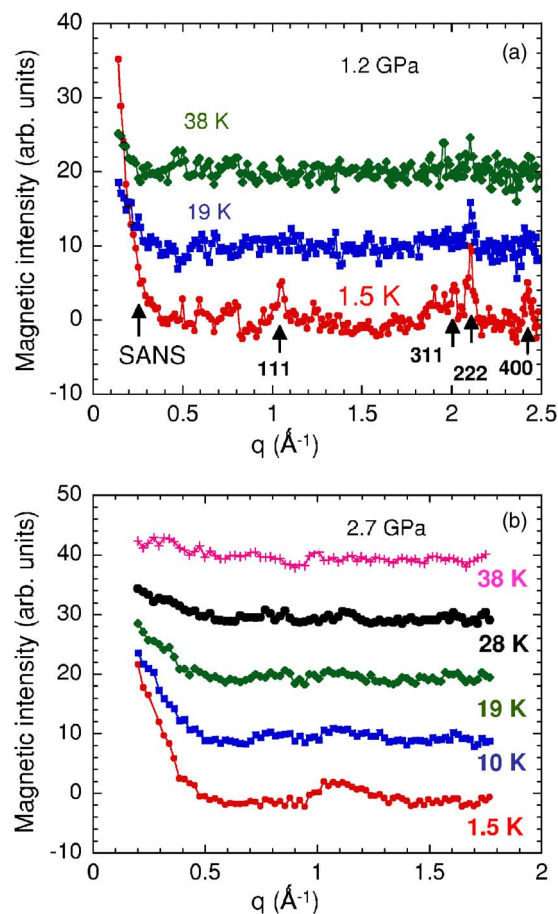


FIG. 10. (Color online) Magnetic diffraction patterns in  $\text{Gd}_2\text{Mo}_2\text{O}_7$  under pressure versus the scattering vector  $q = 4\pi \sin \theta/\lambda$ . (a)  $P=1.2$  GPa; (b)  $P=2.7$  GPa. The diffraction patterns are corrected by a pattern in the paramagnetic range (90 K) and scaled to the nuclear intensity of the (222) Bragg peak.

linear ferromagnetic model, by refining the Bragg peaks using Fullprof. In this procedure, the diffuse scattering and SANS signal were treated as a background. The magnetic peaks were scaled to the nuclear Bragg peak (222) measured in the paramagnetic range. The calculated patterns are shown in Fig. 11(a). The ordered moments are plotted versus pressure in Fig. 11(b). The  $\text{Gd}^{3+}$  moment strongly decreases with increasing pressure. The  $\text{Mo}^{4+}$  moment is expected to decrease too, but being much smaller, its variation is less visible.

To get information about the short range correlations yielding the diffuse magnetic signal at 2.7 GPa, we used the model proposed by Bertaut and Burlet<sup>35</sup> for spin glasses and applied by Greedan *et al.*<sup>36</sup> to the pyrochlore system. A fit of the diffuse magnetic scattering by the sum of radial correlation functions was performed, giving information on the spin-spin correlation parameters  $\gamma$  (Fig. 12). We considered correlations up to the fourth neighbor shell ( $\sim 7.3 \text{ \AA}$ ). The correlation coefficients  $\gamma$  deduced from this fit at 2.7 GPa are plotted in the inset of Fig. 12. The Gd-Gd correlations are  $F$  ( $\gamma_{1,3,4} > 0$ ), while the Gd-Mo are AF ( $\gamma_2 < 0$ ). The AF Mo-Mo correlations responsible for the frustration in the SG state<sup>28</sup> cannot be detected, their contribution being about 50

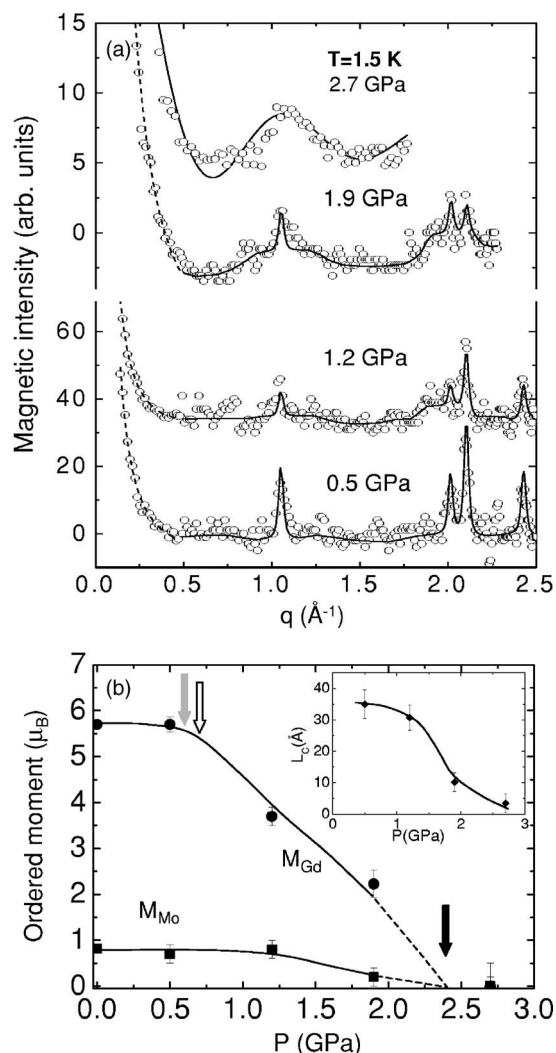


FIG. 11. (a) Magnetic diffraction patterns measured in  $\text{Gd}_2\text{Mo}_2\text{O}_7$  at 1.5 K for several pressures. Solid lines are fits of the Bragg peaks (0.5, 1.2, and 1.9 GPa,  $q > 0.5 \text{ \AA}^{-1}$ ) and of the diffuse peaks (2.7 GPa), respectively. The dashed lines are fits of the SANS signal (0.5, 1.2, and 1.9 GPa,  $q < 0.5 \text{ \AA}^{-1}$ ). All fits are described in the text. (b) Variation of the ordered moments versus pressure. Error bars are given by Fullprof. The arrows indicate the critical pressure as determined from susceptibility (Ref. 14) (0.6 GPa, gray), chemical pressure (Ref. 3) (0.7 GPa, white), and resistivity (Ref. 16) (2.4 GPa, black). In inset: the variation of the correlation length  $L_C$  versus pressure at 1.5 K, as obtained by fitting the SANS with a Lorentzian.

times smaller than the Gd-Gd ones due to the smaller Mo moment.

We outline that in the intermediate pressure range ( $0 < P < 2.7$  GPa) neither the ordered ferromagnetic model nor the short range magnetic model can describe the SANS signal in a proper way. This is because the mesoscopic length scale of the SANS is intermediate between the fourth neighbor shell ( $7 \text{ \AA}$ ) and the domain size associated with the Bragg peaks ( $400 \text{ \AA}$  or above, taking into account the experimental resolution). Considering the relative magnitude of the Mo and Gd local moments and the fact that Mo-Mo and Mo-Gd correlations are AF, we attribute the SANS signal to

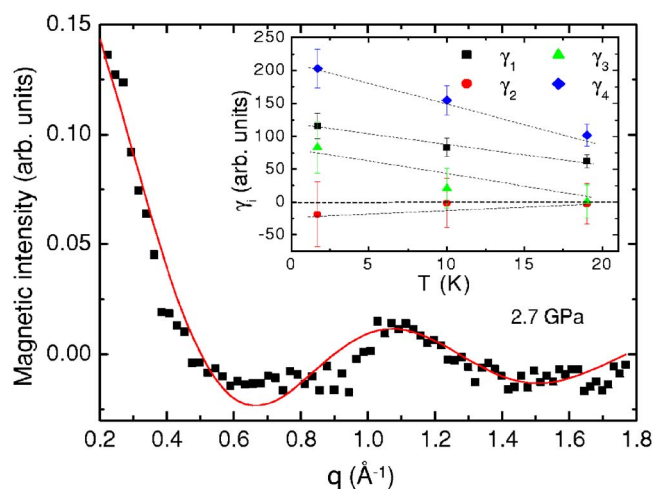


FIG. 12. (Color online) Magnetic intensity in  $\text{Gd}_2\text{Mo}_2\text{O}_7$  at 1.5 K and  $P=2.7$  GPa. The fit is made with the short range model described in the text. In the inset the temperature dependence of the correlation coefficients. Dashed lines are guides to the eye.

ferromagnetic Gd-Gd correlations. To get an insight into their correlation length  $L_C$ , we have fitted the SANS with a Lorentzian function  $A\kappa/[\pi(\kappa^2+q^2)]$  where  $A$  and  $\kappa$  are the norm and half width half maximum of the Lorentzian curve respectively, with  $\kappa=1/L_C$ . The correlation length  $L_C$  is about  $35 \text{ \AA}$  at 0.5 GPa and 1.5 K. It decreases with increasing pressure [inset Fig. 11(b)] and temperature.

## V. DISCUSSION

In this section, we discuss the main results in comparison with other experimental data and existing theories. At ambient pressure, the ordered ground state in  $\text{Gd}_2\text{Mo}_2\text{O}_7$  is a collinear ferromagnet, in contrast with  $\text{Nd}_2\text{Mo}_2\text{O}_7$ , where the  $\text{Nd}^{3+}$  free ion anisotropy induces a spin ice configuration of the  $\text{Nd}^{3+}$  moments.<sup>7,37</sup>

A collinear ground state is expected in  $\text{Gd}_2\text{Mo}_2\text{O}_7$  from the band structure<sup>6</sup> and from the spin only character of  $\text{Gd}^{3+}$  ion. It could explain why there is no giant anomalous Hall effect, in contrast with  $\text{Nd}_2\text{Mo}_2\text{O}_7$ . The ordered magnetic state is, however, strongly abnormal, even at ambient pressure. It coexists with strong fluctuations, which we probe by  $\mu\text{SR}$ , and which persist down to 27 mK according to Mössbauer data.<sup>10</sup> These fluctuations could be responsible for the strong reduction of the ordered moments. The  $\text{Gd}^{3+}$  moment is reduced by 20%, and the  $\text{Mo}^{4+}$  moment by 60% with respect to the free ion values. Spin fluctuations likely play a role in the spin noncollinearity above 20 K. The origin of these fluctuations needs to be clarified. Low temperature collective fluctuations are widely observed in geometrically frustrated magnets and seem to be a key feature of geometrical frustration.<sup>38</sup> However, in  $\text{Gd}_2\text{Mo}_2\text{O}_7$  at ambient pressure, the ferromagnetic Gd-Gd and Mo-Mo first neighbor interactions should be frustrated only by the Gd or Mo anisotropy. This anisotropy is very small, and obviously does not play a key role to select the ground state. A possible source of frustration could come from the Mo orbital degen-

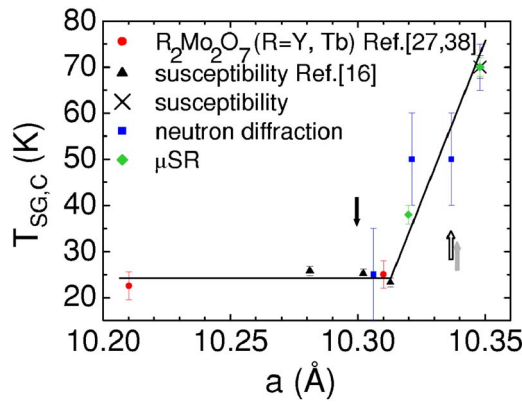


FIG. 13. (Color online) Curie and spin-glass transition temperatures  $T_C$  and  $T_{SG}$  versus lattice constant in  $Gd_2Mo_2O_7$ : (crosses) from susceptibility, (squares) neutron diffraction, and (diamonds)  $\mu$ SR (this work); (triangles) from susceptibility under pressure (Ref. 16). The  $T_{SG}$  values of  $Y_2Mo_2O_7$  ( $a=10.21$  Å) and  $Tb_2Mo_2O_7$  ( $a=10.31$  Å) from Refs. 28 and 40 are plotted for comparison. The arrows indicate the critical lattice constant as determined from susceptibility (Ref. 14) (gray), chemical pressure (Ref. 3) (white), and resistivity (Ref. 16) (black), using our compressibility data.

eracy of the  $t_{2g}$  levels, and the coupling between spin and orbit degrees of freedom.<sup>39</sup> One could also speculate that the abnormal fluctuations come from the proximity of the threshold and the metal-insulating instability. Taking them into account in the band structure is a challenge for theory.

The ferromagnetic state is strongly unstable under pressure, so that a small pressure of 0.5 GPa induces important changes in the magnetic correlations and strongly decreases the  $T_C$  value. Actually in  $Gd_2Mo_2O_7$  our neutron data show that the magnetic order gradually evolves from  $F$  to SG in the pressure range of 0.5–2.5 GPa: in this region, both SG and  $F$  contributions coexist and their relative amounts change with pressure.

Initial measurements in the substituted series<sup>3</sup>  $(RR')_2Mo_2O_7$  support a unique threshold from a ferromagnetic metal to an insulating spin-glass state for a lattice constant  $a_c \sim 10.33$  Å. Using the equation of state found above, it yields a chemical critical pressure of 0.7 GPa. Actually, macroscopic measurements on  $Gd_2Mo_2O_7$  under pressure show a more complex situation. Magnetic measurements under pressure<sup>14,16</sup> suggest a transition from ferromagnetic to spin-glass state already at 0.6 GPa. On the other hand resistivity measurements<sup>16</sup> on *insulating*  $Gd_2Mo_2O_7$  crystals, show that they become metallic at a much higher pressure of 2.4 GPa. It suggests that the ferromagnetic-spin glass transition could be disconnected from the metal-insulating one. We notice that all threshold values belong in the pressure range of coexistence deduced from our neutron data.

In Fig. 13, we have plotted the transition temperature  $T_C$  measured in  $Gd_2Mo_2O_7$  versus the lattice constant, by combining our magnetization, neutron, muon and x-ray data. We also plotted the spin glass transition temperatures  $T_{SG}$  corresponding to the susceptibility anomalies under pressure.<sup>16</sup> These  $T_{SG}$  values are in the temperature range 20–25 K, in good agreement with the values found at ambient pressure in

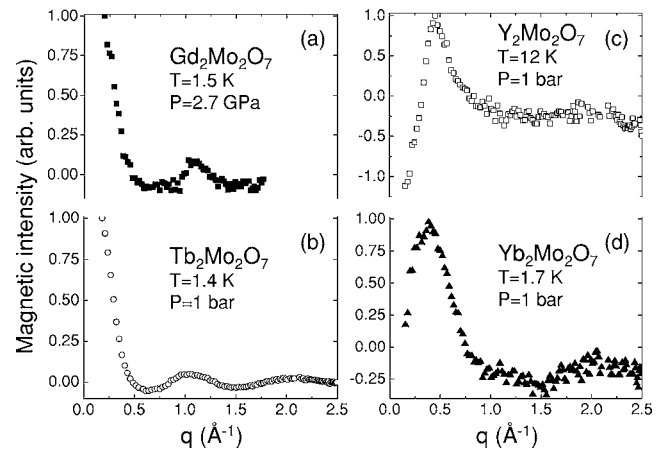


FIG. 14. Magnetic intensity of  $R_2Mo_2O_7$  ( $R=Gd, Tb, Y$ , and  $Yb$ ) versus the scattering vector  $q$ . A pattern in the paramagnetic phase was subtracted.

$Tb_2Mo_2O_7$  and  $Y_2Mo_2O_7$  spin glasses with a smaller lattice constant.<sup>28,40</sup> The temperature for the onset of short range correlations in the spin-glass state is noticeably higher (around 30–40 K at 2.7 GPa) as it often occurs in spin glasses. The whole set of data provides a precise description of the magnetic transition in the instability region.

By comparing the magnetic pattern of  $Gd_2Mo_2O_7$  at 2.7 GPa with patterns of  $R_2Mo_2O_7$  compounds with small ionic radii ( $R=Tb, Y$ , and  $Yb$ ) at ambient pressure, we can get a general insight on the different types of spin correlations in the spin-glass phase. For this purpose we measured the  $Y, Tb$ , and  $Yb$  compounds at ambient pressure (Fig. 14). Our results for  $R=Tb$  and  $Y$  agree with previous results.<sup>28,36,40</sup> We can also follow the evolution of the Mo-Mo, Gd-Mo, and Gd-Gd correlations with pressure from the ferromagnetic to the spin-glass phase.

In the collinear ground state found in  $Gd_2Mo_2O_7$  at ambient pressure, all correlations are ferromagnetic. With increasing pressure, Mo-Mo interactions become AF and frustrated by the lattice geometry yielding the SG phase. Neutron scattering cannot probe the Mo-Mo correlations in the SG phase of  $Gd_2Mo_2O_7$  since their contribution is much smaller than the Gd-Gd and Gd-Mo ones due to the smaller Mo moment. But these correlations can be directly evidenced in  $Y_2Mo_2O_7$  where only the Mo ions are magnetic and the lattice constant ( $a=10.21$  Å from Ref. 28) is equivalent to  $Gd_2Mo_2O_7$  at 6.7 GPa. In  $Y_2Mo_2O_7$ , AF correlations with a scale of about 5 Å forming a four sublattice structure<sup>28</sup> yield a peak in the diffuse scattering at  $q=0.44$  Å<sup>-1</sup>. A similar structure is observed in  $Yb_2Mo_2O_7$  [ $a=10.1689(7)$  Å], where the contribution of the  $Yb^{3+}$  moments (around 1  $\mu_B$ ) is much lower than for  $Tb$  and  $Gd$ .

Concomitantly with the change in the Mo-Mo correlations, the Gd-Mo correlations become AF. The Gd-Gd correlations remain ferromagnetic, but their correlation length decreases with increasing pressure. The comparison of  $Gd_2Mo_2O_7$  with  $Tb_2Mo_2O_7$  suggests that ferromagnetic R-R correlations are a general feature of the  $R_2Mo_2O_7$  series. The length scale of these correlations is reduced by pressure, which enhances the AF interactions. Our measurements on

Tb<sub>2</sub>Mo<sub>2</sub>O<sub>7</sub> under pressure,<sup>41</sup> show that it is also the case for Tb.

From our data, one can evaluate the first neighbor exchange interactions  $\mathcal{J}$  and their contribution to the energy balance. One naturally expects  $\mathcal{J}_{\text{Mo-Mo}} > \mathcal{J}_{\text{Gd-Mo}} > \mathcal{J}_{\text{Gd-Gd}}$ . At ambient pressure, the three interactions are likely all ferromagnetic. Dominant Mo-Mo interactions stabilize the ferromagnetic order but are sensitive to orbital degeneracy and band instability. Gd-Mo ferromagnetic interactions account for the  $F$  alignment of Gd and Mo moments. Gd-Gd interactions cannot be measured. One can speculate that their ferromagnetic character stabilizes the collinear state at low temperature.

We first estimate the exchange energy per ion (Mo or Gd) for the three interactions. For the Mo-Mo exchange, one can state that  $E_{\text{Mo-Mo}} \sim T_C \sim \theta_{\text{CW}} = -70$  K where  $\theta_{\text{CW}}$  is the Curie-Weiss constant. For the Gd-Mo exchange, we use the exchange field acting on Gd, determined by fitting the temperature dependence of the ordered Gd moment (Fig. 5):  $H_{\text{ex}} = 10.8$  T; then:  $E_{\text{Gd-Mo}} = -M_{\text{Gd}} H_{\text{ex}} \sim -45$  K. Finally, to estimate the order of magnitude of the Gd-Gd exchange/dipole energy, we use the  $\theta_{\text{CW}}$  value in Gd<sub>2</sub>Ti<sub>2</sub>O<sub>7</sub> or Gd<sub>2</sub>Sn<sub>2</sub>O<sub>7</sub>, where there is no  $3d/4d$  magnetic metal ion:  $E_{\text{Gd-Gd}} \sim -10$  K. Thus Gd-Mo and Gd-Gd interactions may play a role to determine the ground state in the ferromagnetic phase and threshold region.

In order to estimate the exchange integrals, we make the following assumptions: the exchange between a pair of ions  $A$  and  $B$  is written  $E_{\text{ex}} = -\mathcal{J}_{\text{A-B}} S_A S_B$ , where  $S_A$  and  $S_B$  are the true spins of the  $A$  and  $B$  ions. Then, the exchange energy per ion is  $E_{\text{A-B}} = -z \mathcal{J}_{\text{A-B}} S_A S_B$ , where  $z$  is the number of nearest neighbors ( $z=6$  in the pyrochlore lattice for all exchange bonds). Although an ionic description is not fully appropriate for the Mo ion in Gd<sub>2</sub>Mo<sub>2</sub>O<sub>7</sub>, we assume  $S=1$  for Mo, and for Gd<sup>3+</sup>, we use  $S=7/2$  as there is no crystal field splitting. Then, we obtain the following exchange integrals:  $\mathcal{J}_{\text{Mo-Mo}} \sim 12$  K,  $\mathcal{J}_{\text{Gd-Mo}} \sim 2$  K, and  $\mathcal{J}_{\text{Gd-Gd}} \sim 0.14$  K.

Under applied pressure, we find that the Mo-Mo exchange interaction changes sign and become AF. Calculated phase diagrams for given values of the exchange interactions<sup>36</sup> show that AF Mo-Mo interactions may stabilize a degenerate ground state whatever the sign of the Gd-Mo interactions. Mo-Mo interaction involves Mo  $t_{2g}$  orbitals, which are very sensitive to electron correlations. Pressure is expected to increase the intrasite electron correlation energy  $U$ . At ambient

pressure, our estimation of  $\mathcal{J}_{\text{Mo-Mo}}$  (12 K) is lower than the theoretical estimation of about 5 meV (58 K), obtained by Solov'yev<sup>6</sup> in the mean field Hartree-Fock approach, taking the onsite Coulomb interaction  $U=2.5$  eV between Mo( $4d$ ) electrons. The model predicts that  $\mathcal{J}_{\text{Mo-Mo}}$  strongly decreases as  $U$  increases, although it does not change sign as in Y<sub>2</sub>Mo<sub>2</sub>O<sub>7</sub>. Gd-Gd interactions between localized Gd moments are expected to be less sensitive to pressure.

The change in sign of the Mo-Mo interaction is connected with the aperture of a Mott-Hubbard gap in the Mo  $t_{2g}$  band, so that theory<sup>6</sup> predicts the spin glass state to be insulating. That is actually true for the spin glasses with small ionic radii ( $R=Y, \text{Ho, Dy}$ ), but not for the pressure induced spin-glass state. Resistivity measurements<sup>16,42</sup> in Gd<sub>2</sub>Mo<sub>2</sub>O<sub>7</sub> and Sm<sub>2</sub>Mo<sub>2</sub>O<sub>7</sub> show that the spin-glass state induced under pressure is actually metallic. With respect to chemical pressure, an applied pressure should not only increase the electron correlations responsible for the Mott-Hubbard gap, but also increase the bandwidth. This should naturally favor electron delocalization as a dominant feature. Optical measurements could also check the evolution of conduction properties under pressure.

## VI. CONCLUSION

We have observed an abnormal ferromagnetic phase with strong spin fluctuations in Gd<sub>2</sub>Mo<sub>2</sub>O<sub>7</sub>. By applying pressure, we can tune the change of this ferromagnetic phase into a spin-glass phase. The fact that an applied pressure is equivalent to a chemical pressure to induce the ferromagnetic spin-glass transition supports a mechanism mostly controlled by Mo-Mo interactions. The combination of three microscopic probes under pressure allows us to follow the evolution of magnetism with the lattice constant with great precision throughout the threshold and to evaluate the role of the rare earth interactions in the energy balance.

## ACKNOWLEDGMENTS

We thank U. Zimmerman for the  $\mu$ SR measurements on GPD (PSI) and M. Mezouar for the x-ray measurements on ID27 (ESRF). We are indebted to J. Rodríguez-Carvajal for many useful discussions and for providing programs to analyze the neutron diffraction data. We also thank I. Solov'yev for an interesting discussion.

<sup>1</sup>S. T. Bramwell and M. J. P. Gingras, *Science* **294**, 149 (2001).

<sup>2</sup>J. E. Greedan, *J. Mater. Chem.* **11**, 37 (2001).

<sup>3</sup>T. Katsufuji, H. Y. Hwang, and S.-W. Cheong, *Phys. Rev. Lett.* **84**, 1998 (2000).

<sup>4</sup>Y. Moritomo, S. Xu, A. Machida, T. Katsufuji, E. Nishibori, M. Takata, M. Sakata, and S. W. Cheong, *Phys. Rev. B* **63**, 144425 (2001).

<sup>5</sup>J. S. Kang, Y. Moritomo, S. Xu, C. G. Olson, J. H. Park, S. K. Kwon, and B. I. Min, *Phys. Rev. B* **65**, 224422 (2002).

<sup>6</sup>I. V. Solov'yev, *Phys. Rev. B* **67**, 174406 (2003).

<sup>7</sup>Y. Taguchi, Y. Oohara, H. Yoshizawa, N. Nagaosa, and Y. Tokura, *Science* **291**, 2573 (2001).

<sup>8</sup>Y. Taguchi, T. Sasaki, S. Awaji, Y. Iwasa, T. Tayama, T. Sakakibara, S. Iguchi, T. Ito, and Y. Tokura, *Phys. Rev. Lett.* **90**, 257202 (2003).

<sup>9</sup>N. P. Raju, E. Gmelin, and R. K. Kremer, *Phys. Rev. B* **46**, 5405 (1992).

<sup>10</sup>J. A. Hodges *et al.*, *Eur. Phys. J.: Appl. Phys.* **33**, 173 (2003).

<sup>11</sup>J. E. Greedan, M. Sato, Naushad Ali, and W. R. Datars, *J. Solid State Chem.* **68**, 300 (1987).

- <sup>12</sup>W. Schnelle and R. K. Kremer, *J. Phys.: Condens. Matter* **16**, S685 (2004).
- <sup>13</sup>I. Kézsmárki, N. Hanasaki, D. Hashimoto, S. Iguchi, Y. Taguchi, S. Miyasaka, and Y. Tokura, *Phys. Rev. Lett.* **93**, 266401 (2004).
- <sup>14</sup>J. G. Park *et al.*, *Physica B* **328**, 90 (2003).
- <sup>15</sup>K. Miyoshi, Y. Takamatsu, and J. Takeuchi, *J. Phys. Soc. Jpn.* **75**, 065001 (2006).
- <sup>16</sup>N. Hanasaki, M. Kinuhara, I. Kezsmarki, S. Iguchi, S. Miyasaka, N. Takeshita, C. Terakura, H. Takagi, and Y. Tokura, *Phys. Rev. Lett.* **96**, 116403 (2006).
- <sup>17</sup>D. Schmitt and B. Ouladiaff, *J. Appl. Crystallogr.* **31**, 620 (1998).
- <sup>18</sup>J. Rodríguez-Carvajal, *Physica B* **192**, 55 (1993). For a recent version of Fullprof, see: CPD Newsletters **26**, 12 (2001), available at <http://journals.iucr.org/iucr-top/comm/cpd/newsletters>
- <sup>19</sup>E. F. Bertaut, *Acta Crystallogr., Sect. A: Cryst. Phys., Diffr., Theor. Gen. Crystallogr.* **24**, 217 (1969).
- <sup>20</sup>Y. A. Izyumov, V. E. Naish, and R. P. Ozerov, *Neutron Diffraction on Magnetic Materials* (Consultants Bureau, New York, 1991).
- <sup>21</sup>J. Rodríguez-Carvajal, BasIreps, URL: <ftp://ftp.cea.fr/pub/llb/divers/BasIreps>
- <sup>22</sup>J. D. M. Champion, S. T. Bramwell, P. C. W. Holdsworth, and M. J. Harris, *Europhys. Lett.* **57**, 93 (2002).
- <sup>23</sup>S. E. Palmer and J. T. Chalker, *Phys. Rev. B* **62**, 488 (2000).
- <sup>24</sup>K. Tomala, G. Czjzek, J. Fink, and H. Schmidt, *Solid State Commun.* **24**, 857 (1977).
- <sup>25</sup>E. Dormann, in *Handbook on the Physics and Chemistry of Rare Earths*, edited by K. A. Gschneider, Jr. and L. Eyring (Elsevier, New York, 1991).
- <sup>26</sup>P. Dalmas de Réotier, P. C. M. Gubbens, and A. Yaouanc, *J. Phys.: Condens. Matter* **16**, S4687 (2004).
- <sup>27</sup>P. Dalmas de Réotier and A. Yaouanc, *Phys. Rev. B* **52**, 9155 (1995).
- <sup>28</sup>J. S. Gardner, B. D. Gaulin, S. H. Lee, C. Broholm, N. P. Raju, and J. E. Greedan, *Phys. Rev. Lett.* **83**, 211 (1999).
- <sup>29</sup>P. Bonville *et al.*, *Hyperfine Interact.* **156-157**, 103 (2004); Proceedings of the XXXVIII Zakopane School of Physics, edited by E. Görlich, K. Krolas, A. Pedziwiatr (Institute of Physics, Krakow, Poland, 2003), p. 53.
- <sup>30</sup>F. Bert, P. Mendels, A. Olariu, N. Blanchard, G. Collin, A. Amato, C. Baines, and A. Hillier, *Phys. Rev. Lett.* **97**, 117203 (2006).
- <sup>31</sup>P. Dalmas de Réotier *et al.*, *Phys. Rev. Lett.* **96**, 127202 (2006).
- <sup>32</sup>S. R. Dunsiger *et al.*, *Phys. Rev. B* **54**, 9019 (1996).
- <sup>33</sup>A. Apetrei, I. Mirebeau, I. Goncharenko, D. Andreica, and P. Bonville, *Phys. Rev. Lett.* (to be published), e-print cond-mat/0604627.
- <sup>34</sup>I. Goncharenko, *Rev. High Pressure Sci. Technol.* **24**, 193 (2004).
- <sup>35</sup>E. F. Bertaut and P. Burlet, *Solid State Commun.* **5**, 279 (1967).
- <sup>36</sup>J. E. Greedan, J. N. Reimers, C. V. Stager, and S. L. Penny, *Phys. Rev. B* **43**, 5682 (1991).
- <sup>37</sup>Y. Yasui *et al.*, *J. Phys. Soc. Jpn.* **72**, 865 (2003).
- <sup>38</sup>S. Bramwell *et al.*, *Phys. Rev. Lett.* **87**, 047205 (2001).
- <sup>39</sup>M. W. Kim, Y. S. Lee, T. W. Noh, J. Yu, and Y. Moritomo, *Phys. Rev. Lett.* **92**, 027202 (2004).
- <sup>40</sup>B. D. Gaulin, J. N. Reimers, T. E. Mason, J. E. Greedan, and Z. Tun, *Phys. Rev. Lett.* **69**, 3244 (1992).
- <sup>41</sup>A. Apetrei, I. Mirebeau, I. Goncharenko, D. Andreica, and P. Bonville, *Proceedings of the International Conference on Highly Frustrated Magnetism*, edited by Z. Hiroi and H. Tsunetsugu, *J. Phys.: Condens. Matter* (HFM2006, Osaka, Japan), to be published.
- <sup>42</sup>K. Miyoshi, T. Yamashita, K. Fujiwara, and J. Takeuchi, *J. Phys. Soc. Jpn.* **72**, 1855 (2003).